2013 International Conference on Renewable Energy Research and Applications (ICRERA)

Programme

Control of Wind Power

Péter Nagy, Péter Stumpf, István Nagy
Budapest University of Technology and Economics
Department of Automation and Applied Informatics
Budapest, Hungary
nagy@get.bme.hu

***Abstract* — The paper is concerned with the Wind Energy Converter System applying Doubly Fed Induction Generator. It treats the control of Rotor Side Converter when the stator flux oriented vector control strategy is used. The relations are derived governing the stator and rotor power flow and the electric torque controlled by the d and q component of the rotor supply voltage. The relations are illustrated by characteristics in per unit and their evaluations throw light to the physical background with practical application comments. The description is devised in a comprehensive and concise way.**

Keywords: wind power, control of doubly fed induction generator, torque-speed characteristics, torque-power characteristics.

I. INTRODUCTION

One of the greatest challenges for human kind is to secure the soaring energy demand and avoiding the climate change. Renewable energies are promising players in the future energy sources. The renewable energies are planed to take part in the solution of energy crisis.

The major renewable energy sources are the wind, photovoltaic (PV), hydro, biomass, tidal and wave etc. energies. We are interested in the paper in the utilization of wind energy. The wind energy installations are growing exponentially in developed countries and intensive research is supported by governments and industries. Fig.1 shows the global installed cumulative wind capacity (ICWC) from 1996 to 2010. The new, added capacity was approximately 27 GWs in 2008 and 37 GWs in 2009. The annual market growth was more than 35%

Now the total cumulative wind capacity is well over 200 GWs. The ICWC was about the same, approximately 40 GWs in Nord America and in Asia in 2009, while its value was almost twice as high, 76 GWs in Europe.

The paper is concerned with the study of wind energy conversion system (WECS) and in particular the modeling and control of the doubly fed induction generator (DFIG) connected to the grid within WECS. Its performance and control is quite different from the conventional induction generator. Its comprehensive and concise description together with characteristics in per unit is not readily available in the relevant literature. The results presented here offer better insight both into the steady-state and dynamic performance of the system.

The sections are organized as follows: Section II briefly describes the WECS with DFIG and Section III discusses its control. Section IV derives the relations for the stator power flow when stator flux oriented vector control is applied in the rotor side converter. Section V contains the slip-torque and slip-stator reactive power curves and their evaluations. The Conclusions are in Section VI. The derivations of the relations used in the paper are in the Appendix.

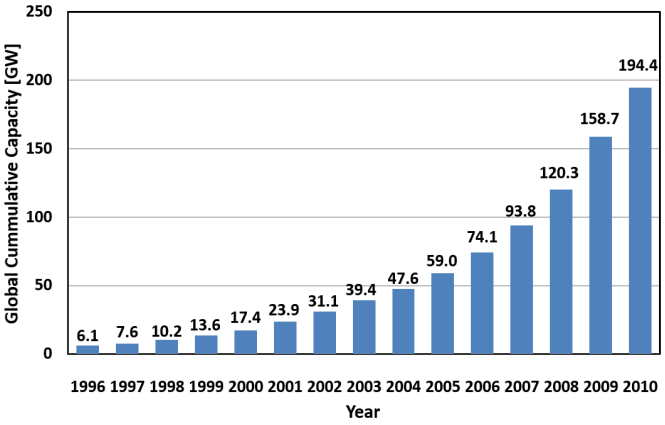

Fig. 1 Global installed commulative wind capacity (soruce: Global Wind Energy Council)

II. DOUBLY-FED INDUCTION GENERATOR (DFIG) IN WECS

Currently the most popular WECSs apply DFIG. Technical and economic reasons explain the widespread application of this configuration. It incorporates two three phase converters; both are seated in the rotor circuit between the rotor terminals of IG and the grid (Fig.2).

DC link connects the rotor side converter (RSC) and the grid side converter (GSC). The stator of DFIG is directly connected to the grid. The generator is driven through gear box by the wind turbine operating in a speed range (6~20) rpm. The synchronous speed of IG is (1000-1500) rpm for a 6 or 4 pole IG, therefore high conversation ratio is needed for coupling the turbine and the generator.

± 30% of speed range around the synchronous speed of IG is usually satisfactory to harvest the optimum wind power up to rated wind velocity by controlling the speed of the turbine-generator set and independently the power factor. The speed change within this speed range can be done by the rotor supply voltage. There are decisive benefits from the greatly reduced speed range. The weight, volume and investment cost of the two converters, the RSC and GSC are only a fraction of those designed for full rated power as their rated power is only the third of the rated power of the generator or to the rated power

978-1-4799-1464-7/13/$31.00 ©2013 IEEE

of the full-capacity converters connected in series in the stator circuit. Similarly the power loss is substantially lowered in the two converters and the efficiency of the overall system is boosted.

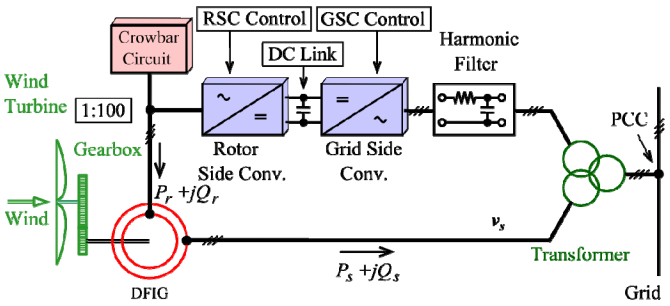

Fig. 2 Wind energy conversion system (WECS) with DFIG

The converters with the DC link partly decouple the wind turbine and the grid and they make it possible to supply power to the grid working at constant voltage and frequency while the rotor speed varies ± 30%. As the DFIG works both in subsynchronous and supersynchronous state the power flow is bidirectional in the rotor. The largest drawbacks in the WECS with DFIG are the slip rings. The reliability of WECS depends on it. As most WECS installed apply DFIG the paper is concerned exclusively with this system.

III. Controls in WECS Applying Doubly Fed Induction Generator (DFIG)

The short overview of the controls in WECS with DFIG can be divided into two parts: Turbine side controls and Generator side controls. The controls in the turbine side consist of pitch control and yaw control. The pitch mechanism performs the rotation of the three blades of the turbine on their longitudinal axis. The angle of attack of the blades is modified by the rotation and it affects the captured wind power and the power conversion efficiency. They can be optimized by pitch control. It even offers protection of the turbine structure against damage caused by strong wind.

The other turbine side control is the yaw control which keeps the area swept by the blades facing always into the directions of the wind maximizing the captured wind power.

The generator side controls are performed by the RSC and the GSC. The RSC control regulates the stator active and reactive power by rotor current component i_{dr} and i_{qr}, respectively. It can be expressed in another way. The stator active and reactive power can be modified by the two components of rotor supply voltage: v_{dr} and v_{qr} (See details later).

Finally the GSC control regulates the DC link voltage in the rotor circuit and the rotor reactive power flow Q_r between GSC and the grid by the grid side rotor current component i_d and i_q. (i_d and i_q are different from i_{dr} and i_{qr}). Regulating the DC link voltage modifies the P_r active power of the rotor.

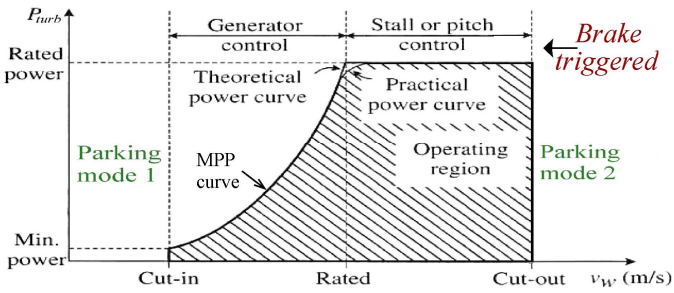

Fig. 3 Turbine power P_{turb} as a function of wind speed v_w. Four operation modes.

Fig. 3 presents the turbine power P_{turb} as a function of wind speed v_w. The operation modes are classified in four modes in the wind speed range In the "Parking Mode1" below the so called Cut-in wind speed the turbine generator set is turned-off, it is in stall. The captured power P_{turb} would be less than the loss of the system. Above the Cut-out wind speed in "Parking Mode2" the wind turbine is stopped again ($\omega_{turb} = 0$) to prevent the mechanical damage resulting in very high wind. The "Generator Control section" starts from the Cut-in wind speed to the rated wind speed or $\omega_{turb} = 1$ p.u. The Maximum Power Point Tracking (MPPT) control sets ω_{turb} at the peak power point (MPP) of each wind speed. Along the trajectory of MPP curve P_{turb} is proportional to ω^3_{turb}. Finally in the "Pitch Control section" the harvested power is kept at $P_{turb} = 1$ p.u. to avoid higher mechanical and electrical stress than their rated values. As it has been mentioned the stator and the rotor active and reactive power can be controlled by RSC. The paper treats in next sections in some detail the RSC control.

IV. Power Flow

The direction of the active power flow is always from the turbine to the generator and from the generator to the grid through the stator but bidirectional power flow can take place in the rotor circuit. The stator flux oriented vector control (SFOVC) is the most popular control strategy in the RSC. Next we have an insight how the electric torque T_e and generator speed or slips s can be changed by the rotor supply voltage $\boldsymbol{V}_r$, or current $\boldsymbol{I}_r$ space vectors applying SFOVC in steady-state. It opens the door for the determination of the active and reactive power flow both in the stator and in the rotor. All vectors are space vectors in the paper. In this study the stator copper, iron and ventilation losses are neglected.

In the stator flux oriented vector control the basic equations are written in Rotating Reference Frame (RRF) revolving with synchronous angular speed ω_s determined by the stator frequency f_s. The stator flux oriented vector control means that the d axis of RRF is fixed to space vector of the stator linkage flux $\boldsymbol{\Psi}_s$ (Fig. 4). Therefore $\Psi_{qs} = 0$. Considering steady-state, the grid voltage $\boldsymbol{V}_s$ and its angular frequency ω_s are assumed constant. Neglecting the stator resistance ($R_s = 0$), $\boldsymbol{V}_s = j\omega_s \boldsymbol{\Psi}_{ds} = j\boldsymbol{V}_{qs}$. Both $\boldsymbol{\Psi}_s = \boldsymbol{\Psi}_{ds}$ and V_{qs} are constant and $V_{ds} = 0$.

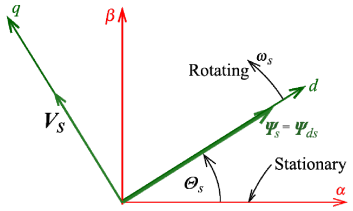

Fig. 4 Stationary and Rotating Reference Frame

The basic equations are derived in Appendix 1. From now on steady-state is considered, capital letters are used instead of lower case and we take into account $V_{qs} = R_s I_{qs} + \omega_s \Psi_{ds} \approx \omega_s \Psi_{ds} = V_s$ from (A1.4). V_s is the absolute value of the stator voltage space vector or that of the grid voltage.

Substituting V_{ds} from (A1.3) and V_{qs} from (A1.4) into relation (A1.14) the stator active power in steady-state is

$$P_s = \frac{3}{2}\left(\Psi_{ds} I_{qs} - \Psi_{qs} I_{ds}\right)\omega_s = T_e \omega_s \tag{1}$$

where T_e is the electric torque. Applying $\Psi_{qs} = 0$ and $V_{qs} = \omega_s \Psi_{ds}$, the stator active power from (A1.10) and (1) is

$$P_s = \frac{3}{2} V_{qs} I_{qs} = \frac{3}{2}\frac{L_m}{L_s} V_{qs} I_{qr} = K_p I_{qr} \tag{2}$$

and the stator reactive power from (A.1.15) and (A1.9)

$$Q_s = \frac{3}{2} V_{qs} I_{ds} = \frac{3}{2} V_{qs} \frac{1}{L_s}(\Psi_{ds} + L_m I_{dr}) = K_{Q1} + K_{Q2} I_{dr} \tag{3}$$

Applying (1) and (A1.10), the electric torque is

$$T_e = \frac{3}{2}\Psi_{ds} I_{qs} = \frac{3}{2}\frac{L_m}{L_s}\Psi_{ds} I_{qr} \tag{4}$$

Equation $\Psi_{qs} = 0$ and $I_{qs} = (L_m/L_s)\, I_{qr}$ is taken into account in (2) and (4) from (A1.10). Equation $I_{ds} = (1/L_s)\,(\Psi_{ds} + L_m I_{dr})$ from (A1.9) is used in (3). The main message from (2) and (3) is that both the stator active power P_s and the reactive power Q_s can be changed independently by the rotor current component I_{qr} and I_{dr}, respectively. Furthermore the torque can be changed together with P_s by I_{qr}.

V. TORQUE AND STATOR POWER RELATIONS

Both the stator active power and the torque can be varied by I_{qr} [(2) and (4)] in steady-state as it is expected. The torque-slip relation $T_e(s)$ is derived in Appendix 2:

$$T_e(s) = \frac{3}{2}\frac{X_m}{X_s}\frac{(\sigma s) V_s V_{dr} - \left(\frac{R_r}{X_r}\right) V_s V_{qr} + s\left(\frac{R_r}{X_r}\right)\left(\frac{X_m}{X_s}\right) V_s^2}{\omega_s X_r\left[\left(\frac{R_r}{X_r}\right)^2 + \sigma^2 s^2\right]} \tag{5}$$

Knowing $T_e(s)$, the stator active power versus slip $P_s(s)$ in steady-state is known as well ($R_s = 0$)

$$P_s(s) = \omega_s T_e \tag{6}$$

Using the extreme value calculation by the slip derivative of (5), the slip value belonging to peak torque is

$$s_{+,-}^{peak} = s_0 \pm \sqrt{s_0^2 + \left(\frac{R_r}{X_r}\right)^2 \frac{1}{\sigma^2}} = s_0 \pm \Delta s^{peak} \tag{7}$$

where s_0 is the slip belonging to $T_e = 0$. Its value from (5) is

$$s_0 = \frac{\frac{X_s}{X_m}\frac{V_{qr}}{V_s}}{1 + \sigma \frac{X_r}{R_r}\frac{X_s}{X_m}\frac{V_{dr}}{V_s}} \tag{8}$$

With the numerical values given in Appendix 3 $s_{+,-}^{peak} = \pm 0.051$ when $V_{qr} = 0$ and it is independent of V_{dr}. In the case when $V_{dr} = 0$

$$s_{+,-}^{peak} = \frac{X_s}{X_m}\frac{V_{qr}}{V_s} \pm \sqrt{\left(\frac{X_s}{X_m}\frac{V_{qr}}{V_s}\right)^2 + \left(\frac{R_r}{X_r}\right)^2 \frac{1}{\sigma^2}} \tag{9}$$

The slope dT_e/ds at $s = 0$ depends on the sign of V_{dr} and it is always positive when $V_{dr} \geq 0$. The sign of the slope is crucial as it determines the stability in the lack of feedback control. The slope can be negative by negative V_{dr}. In the border case the slope is zero, $dT_e/ds = 0$ and it occurs when the voltage

$$V_{dr0} = -\frac{R_r}{X_r}\frac{X_m}{X_s}\frac{1}{\sigma} V_s \tag{10}$$

which can be derived from (6). Using the numerical values given in Appendix 3, $V_{dr0} = -0.0492$ p.u. is obtained.

On the basis of (6) the slip-torque characteristics are drawn first when the parameter is V_{qr} and V_{dr} is zero (Fig. 5) and conversely when the parameter is V_{dr} and V_{qr} is zero (Fig. 6), respectively. The numerical values used for the calculation are listed in Appendix 4.

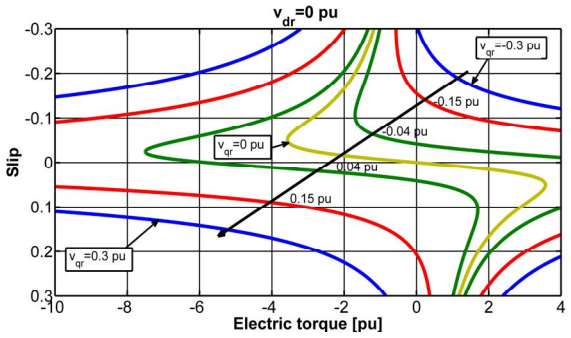

Fig. 5 Slip-torque characteristics. Paramter V_{qr}. Voltage component $V_{dr} = 0$

The rated working area in steady-state is stretched along the slip axis from $s = 0.3$ to $s = -0.3$ and in the torque axis from $T_e = 0$ to $T_e = -1$ p.u.. In transient state (e.g. having a short circuit in the network) the operation area in the torque axis can be much larger in absolute value (4-6 times larger or more).

The following conclusions can be drawn from Fig. 5:

1.) The speed, or slip can be changed in much wider range by V_{qr} than by V_{dr} at constant T_e in the stable part of $s(T_e)$. See Fig. 6.

2.) Depending on the sign of voltage V_{qr}, the slip s_0 belonging to $T_e = 0$ can be positive or negative and the $s(T_e)$

curves are shifted by V_{qr} in vertical direction. On the other hand, if the slip has to be changed in large step from $s = 0$ to $s = \pm 0.3$ the voltage change needed in negative slip direction is $V_{qr} = -0.3$ p.u. and in positive slip direction $V_{qr} = 0.2$.

3.) The slope dT_e/ds of all curves are positive at the crossing points when $T_e = 0$ in the range $|s| \leq 0.3$. The crossing points are in the stable segments of the curves.

4.) The peak torques T_e^{peak} are placed on both sides of s_0 shifted by $\pm\Delta s^{peak}$ (see (8)). The negative T_e^{peak} is shifted by $-\Delta s^{peak}$ and conversely the positive T_e^{peak} is shifted by $+\Delta s^{peak}$ around s_0.

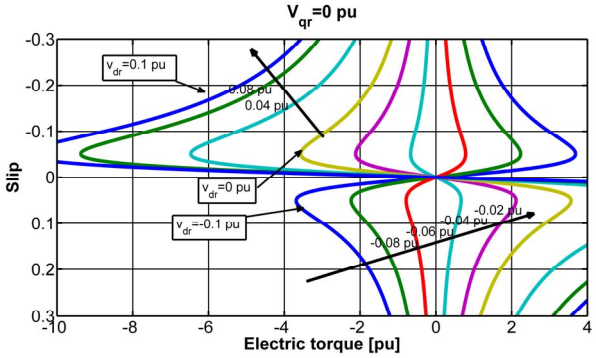

Fig. 6 Slip-torque characteristics. Paramter V_{dr}. Voltage component $V_{qr} = 0$

Next the characteristics $s(T_e)$ with $V_{qr} = 0$ are treated (Fig. 6). Now the parameter is V_{dr}. All curves are crossing the point $s = 0$, $T_e = 0$. The speed, slip can be changed in a very narrow band in the stable segments of the curves by voltage V_{dr}. Stable segments of curves $s(T_e)$ exist for positive V_{dr}. When V_{dr} is more negative than $V_{dr0} = -0.0492$ p.u. the slope dT_e/ds turns to negative value at $s = 0$, where $s(T_e)$ is unstable. The conclusion is that the component V_{dr} as control signal for changing the speed is not practical.

Turning to the stator reactive power flow in the stator, the starting equation from (4) for deriving the stator reactive power versus slip, $Q_s(s)$ is

$$Q_s = \frac{3}{2}\frac{V_s}{X_s}(V_s + X_m I_{dr}) \tag{11}$$

where $V_{qs} \approx \omega_s \Psi_{ds} \approx V_s$ was used (see (A1.4)). Substituting I_{dr} from (A2.2) and I_{qr} from (A2.4) into (12), we end up with

$$Q_s = \frac{3}{2}\left\{\frac{V_s^2}{X_s} - \frac{X_m}{X_s}\frac{V_s V_{dr}}{R_r} + \left[\frac{V_s^2}{X_r}\frac{X_m}{X_s}s + \frac{V_s V_{dr}}{R_r}\omega s - \frac{V_s V_{qr}}{X_r}\right] \cdot \frac{(X_m / X_s)\omega s}{(R_r / X_r)^2 + (\omega s)^2}\right\} \tag{12}$$

On the basis of (13) the characteristics of $s(Q_s)$ are drawn in Fig. 7. The curves are image reflected by mirror to axis $s = 0$. All curves are crossing point $s = 0$, $Q_s = (3/2)V_s^2/X_s$ when $V_{dr} = 0$ (Fig. 7b). At constant speed Q_s can be changed either by V_{dr} (Fig. 7a) or by V_{qr} (Fig. 7b.) except $s = 0$, where only V_{dr} can change Q_s. The velocity of change in Q_s when both s and V_{qr} are constant

$$G_{V_{dr}} = \frac{dQ_s}{dV_{dr}} = \frac{3}{2}\frac{V_s}{R_r}\left[\frac{(X_m / X_s)(\omega s)^2}{(R_r / X_r)^2 + (\omega s)^2} - \frac{X_m}{X_s}\right]_{s=const, V_{qr}=const} \tag{13}$$

and when both s and V_{dr} are constant

$$G_{V_{qr}} = \frac{dQ_s}{dV_{qr}} = \frac{3}{2}\frac{V_s}{X_r}\left[\frac{(X_m / X_s)\omega s}{R_r / X_r + (\omega s)^2}\right]_{s=const, V_{dr}=const} \tag{14}$$

Table I. shows G_{Vdr} and G_{Vqr} at different slip values. G_{Vdr} is always negative, it does not depend on V_{dr} and on the sign of s and symmetrical to axis s. It depends on V_{dr} only on s. G_{Vqr} is negative for $s > 0$ and conversely it is positive for $s < 0$. Otherwise its absolute values are the same for the same $|s|$. Around zero slip $|G_{Vdr}|$ is much higher than $|G_{Vqr}|$ and as $|s|$ is getting larger it turns around, $|G_{Vqr}|$ becomes higher.

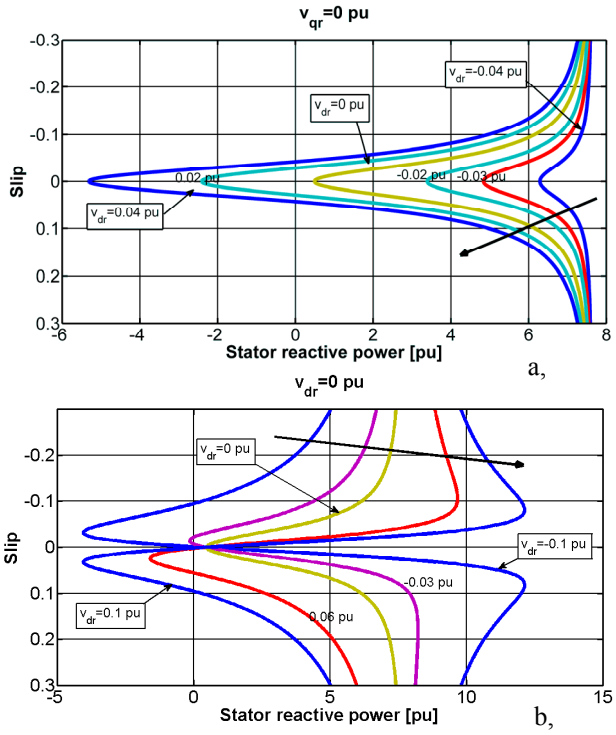

Fig. 7 Slip versus stator reactive power, $s(Q_s)$ curves. parameter V_{dr} (Fig.7a) and V_{qr} (Fig.7b)

TABLE I

slip	$G_{V_{dr}}$ ($Vqr = 0$)	$G_{V_{qr}}$ ($Vdr = 0$)
-0.25	-5.8	28.33
-0.2	-8.8	134.64
-0.1	-29.79	58.62
0	-145.16	0
0.1	-29.79	-58.62
0.2	-8.8	-34.6
0.25	-5.8	-28.44

VI. CONCLUSIONS

On the basis of stator flux oriented vector control of rotor side converter the relations and characteristics of slip-torque and slip-power of doubly fed induction generator were

derived. The electric torque and stator active power can be controlled by I_{qr} or V_{qr}, while the stator reactive power can be changed by I_{dr} or V_{dr}. It was shown that negative V_{dr} can change the positive sign of the slope into negative one producing unstable region around slip $s = 0$. When the stator and rotor supply voltages are in phase subsynchronous state, when they are phase shifted by 180° super-synchronous state exist.

APPENDIX 1. BASIC RELATIONS

The aim is to derive a few basic relations for doubly fed induction machine (DFIM). Space vectors and Rotating Reference Frame (RRF) fixed to the stator linkage flux space vector $\boldsymbol{\Psi}_s$ are used (Fig. 4). RRF is fixed to vector $\boldsymbol{\Psi}_s$ revolving with angular frequency ω_s.

The stator and rotor voltage equations in space vector form are

$$\boldsymbol{v_s} = -R_s\boldsymbol{i_s} + p\boldsymbol{\Psi_s} + j\omega_s\boldsymbol{\Psi_s} \tag{A1.1}$$

$$\boldsymbol{v_r} = -R_r\boldsymbol{i_r} + p\boldsymbol{\Psi_r} + j(\omega_s - \omega_m)\boldsymbol{\Psi_r} \tag{A1.2}$$

where $\omega_m = P\omega_{mech}$, P = Nr. of pole pairs, $p = d/dt$. v_s, v_r and i_s, i_r are the stator and rotor voltage and current space vectors, respectively. The resistance of one phase is R_s and R_r.

Here ωmech is the rotor mechanical angular frequency. The d and q coordinate equations of eq. (A1.1) and (A1.2), respectively

$$v_{ds} = R_s i_{ds} + p\Psi_{ds} - \omega_s\Psi_{qs} \tag{A1.3}$$

$$v_{qs} = R_s i_{qs} + p\Psi_{qs} + \omega_s\Psi_{ds} \tag{A1.4}$$

$$v_{dr} = -R_r i_{dr} + p\Psi_{dr} - \omega_{slip}\Psi_{qr} \tag{A1.5}$$

$$v_{qr} = -R_r i_{qr} + p\Psi_{qr} + \omega_{slip}\Psi_{dr} \tag{A1.6}$$

The stator and rotor linkage flux equation in space vector form are

$$\boldsymbol{\Psi_s} = L_s\boldsymbol{i_s} - L_m\boldsymbol{i_r} \tag{A1.7}$$

$$\boldsymbol{\Psi_r} = L_m\boldsymbol{i_s} - L_r\boldsymbol{i_r} \tag{A1.8}$$

where L_s and L_r are the stator and rotor inductances, L_m the mutual inductance. The d and q coordinate equations of (A1.7) and (A1.8), respectively

$$\Psi_{ds} = L_s i_{ds} - L_m i_{dr} \tag{A1.9}$$

$$\Psi_{qs} = L_s i_{qs} - L_m i_{qr} \tag{A1.10}$$

$$\Psi_{dr} = L_m i_{ds} - L_r i_{dr} \tag{A1.11}$$

$$\Psi_{qr} = L_m i_{qs} - L_r i_{qr} \tag{A1.12}$$

The instantaneous stator power

$$s_s = p_s + jq_s = \frac{3}{2}\boldsymbol{v_s}\boldsymbol{i_s}^* = \frac{3}{2}\left\{\mathrm{Re}\left[\boldsymbol{v_s}\boldsymbol{i_s}^*\right] + j\,\mathrm{Im}\left[\boldsymbol{v_s}\boldsymbol{i_s}^*\right]\right\} \tag{A1.13}$$

where i_s^* is the complex conjugate of space vector i_s. 3 stands for 3 phases, 2 stands for peak values of v_s and i_s.

Taking into account $v_s = v_{ds} + jv_{qs}$ and $i_s = i_{ds} + ji_{qs}$ the active power p_s and reactive power q_s are

$$p_s = \frac{3}{2}\left(v_{ds}i_{ds} + v_{qs}i_{qs}\right) \tag{A1.14}$$

$$q_s = \frac{3}{2}\left(v_{qs}i_{ds} - v_{ds}i_{qs}\right) \tag{A1.15}$$

Considering that $\Psi_s = \Psi_{ds}$, that is, $\Psi_{qs} = 0$, and substituting the linkage flux equations (A1.11), (A1.12) into the rotor voltage equations (A1.5), (A1.6) the results are

$$v_{dr} = v_{dri}(i_{dr}) + v_{drq}(i_{qr}, \Psi_{ds}) \tag{A1.16}$$

$$v_{qr} = v_{qri}(i_{qr}) + v_{qrd}(i_{dr}; \Psi_{ds}) \tag{A1.17}$$

where

$$v_{dri} = -(R_r + \sigma L_r p)i_{dr} \tag{A1.18}$$

$$v_{drq} = \omega_{slip}\sigma L_r i_{qr} + \frac{L_m}{L_s}p\Psi_{ds} \tag{A1.19}$$

and

$$v_{qri} = -(R_r + \sigma L_r p)i_{qr} \tag{A1.20}$$

$$v_{qrd} = -\omega_{slip}\left[\sigma L_r i_{dr} - \frac{L_m}{L_s}\Psi_{ds}\right] \tag{A1.21}$$

The two stator quantities ids and i_{qs} had been eliminated from (A1.16)…(A1.21) by using the stator flux linkage relation (A1.9), (A1.10) and $\Psi_{qs} = 0$. The value σ is

$$\sigma = 1 - \frac{L_m^2}{L_s L_r} \tag{A1.22}$$

Note, that the term v_{drq} in (A1.16) and v_{qrd} in (A1.17) are expressing cross-coupling between the d and q components as v_{dr} depends not only on i_{dr} but on i_{qr} as well and similarly v_{qr} depends not only on i_{qr} but on i_{dr} as well.

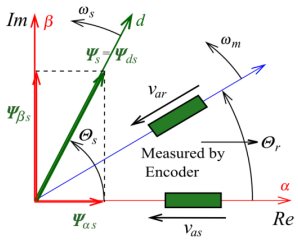

Fig. A.1.1 Determination of Θ_s and ω_s

The determination of angle Θ_s is needed for the calculation of dynamics and for the control of DFIG (Fig.A1.1 and A1.2). In Stationary Reference Frame (SRF) α, β

$$\boldsymbol{v_s} = v_{\alpha s} + jv_{\beta s} \tag{A1.23}$$

$$\boldsymbol{i_s} = i_{\alpha s} + ji_{\beta s} \tag{A1.24}$$

The calculation of the α and β component of the stator flux linkage space vector Ψ_s can be done by

$$\Psi_{\alpha s} = \int\left(v_{\alpha s} - R_s i_{\alpha s}\right)dt \tag{A1.25}$$

$$\Psi_{\beta s} = \int\left(v_{\beta s} - R_s i_{\beta s}\right)dt \tag{A1.26}$$

The instantaneous value of angle Θ_s is (Fig. A1.2)

$$\Theta_s = \tan^{-1}\left(\Psi_{\beta s}/\Psi_{\alpha s}\right) \tag{A1.27}$$

and the angular frequency

$$\omega_s = \frac{d\Theta_s}{dt} \tag{A1.28}$$

APPENDIX 2. TORQUE AND ROTOR POWER RELATIONS

The aim is the derivation of the torque-slip relation. Applying stator flux oriented vector control, the flux component $\Psi_{qs} = 0$. From (A1.10)

$$i_{qs} = \frac{L_m}{L_s}i_{qr} \tag{A2.1}$$

Let us express v_{dr} and v_{qr} [see (A1.5), (A1.6)] as a function of i_{dr} and i_{qr} by substituting Ψ_{dr} and Ψ_{qr} from (A1.11) and (A1.12), respectively

$$v_{dr} = -R_r i_{dr} + \omega_{slip} \sigma L_r i_{qr} \quad \text{(A2.2)}$$

$$v_{qr} = -R_r i_{qr} - \omega_{slip} \left(\sigma L_r i_{dr} - \frac{L_m}{L_s} \Psi_{ds} \right) \quad \text{(A2.3)}$$

Here eq. (A2.1) and (A1.9) were used as well. From the last two equations

$$i_{dr} = \frac{1}{D(s)} \left[-\frac{R_r}{X_r} v_{dr} - \sigma s v_{qr} + \sigma s^2 \frac{X_m}{X_s} V_s \right] \quad \text{(A2.4)}$$

$$i_{qr} = \frac{R_r / X_r}{D(s)} \left\{ -v_{qr} + s \left[(X_r / R_r) \sigma v_{dr} + (X_m / X_s) V_s \right] \right\} \quad \text{(A2.5)}$$

where

$$D(s) = X_r \left[\left(\frac{R_r}{X_r} \right)^2 + (\sigma s)^2 \right] \quad \text{(A2.6)}$$

Here $V_s = \omega_s \Psi_{ds}$ the grid voltage, $X_r = \omega_s L_r$ and $s = \omega_{slip}/\omega_s$ the slip. Substituting i_{qr} from (A2.5) into the torque equation (5) the torque

$$T_e(s) = \frac{3}{2} \frac{X_m}{X_s} V_s i_{qr} = \frac{3}{2} \frac{X_m}{X_s} \frac{R_r / X_r}{D_{(s)}} \cdot \cdot \left\{ -v_{qr} V_s + s \left[(X_r / R_r) \sigma v_{dr} V_s + (X_m / X_s) V_s^2 \right] \right\} \quad \text{(A2.7)}$$

The instantaneous rotor power likewise to stator power (A1.13)

$$s_r = p_r + j q_r = \frac{3}{2} \boldsymbol{v_r}\, \boldsymbol{i_r^*} = \frac{3}{2} \left\{ R_e \left[\boldsymbol{v_r}\, \boldsymbol{i_r^*} \right] + j \,\mathrm{Im} \left[\boldsymbol{v_r}\, \boldsymbol{i_r^*} \right] \right\} \quad \text{(A2.8)}$$

Substituting here $\boldsymbol{v}_r = v_{dr} + j v_{qr}$ and $\boldsymbol{i}_r^* = i_{dr} - j i_{qr}$

$$p_r = \frac{3}{2} \left(v_{dr}\, i_{dr} + v_{qr}\, i_{qr} \right) \quad \text{(A2.9)}$$

$$q_r = \frac{3}{2} \left(v_{qr}\, i_{dr} - v_{dr}\, i_{qr} \right) \quad \text{(A2.10)}$$

APPENDIX 3. NUMERICAL VALUES

	Notation	Value p.u.
Grid voltage	V_s	1
Grid angular frequency	ω_s	1
Stator linkage flux	$\Psi_s = \Psi_{ds}$	1
Mutual inductance	$X_m = L_m$	3
Stator inductance	$X_s = L_s$	3.1
Rotor inductance	$X_r = L_r$	3.1
Stator resistance	R_s	0.01
Rotor resistance	R_r	0.01

$$\sigma = 1 - \frac{L_m^2}{L_s L_r} = 0.0634$$

ACKNOWLEDGMENT

The authors wish to thank the Hungarian Research Fund (OTKA K100275) and the Control Research Group of the Hungarian Academy of Sciences (HAS). This work is connected to the scientific program of the "Development of quality-oriented and harmonized R+D+I strategy and functional model at BME" project. This project is supported by the New Széchenyi Plan (Project ID: TÁMOP-4.2.1/B-09/1/KMR-2010-0002).

REFERENCES

[1] Maurício B. C. Salles , Kay Hameyer , José R. Cardoso , Ahda. P. Grilo and Claudia Rahmann "Crowbar System in Doubly Fed Induction Wind Generators" Energies 2010, 3, 738-753

[2] J. Wang, J. Zhang, Y Zhong, „Study on a Super Capacitor Energy Storage System for Improving the Operating Stability of Distributed Generation System" Conference on Electric Utility Deregulation and Restructuring and Power Technologies, 2008, DRPT 2008, Nanjing, China, 6-9 April 2008, pp. 2702 – 2706

[3] Sergey Ryvkin, „Elimination of the Voltage Oscillation Influence in the 3-Level VSI Drive Using Sliding Mode Control Technique", AUTOMATIKA, 51(2), 2010, pp. 138-148

[4] L. Benadero, V. Moreno-Font, R. Giral, A. El Aroudi, "Topologies and Control of a Class of Single Inductor Multiple-Output Converters Operating in Continuous Conduction Mode", IET Power Electronics, Vol. 4, No. 8, pp. 927-935, 2011

[5] J. Leuchter, P. Bauer, V. Rerucha, V. Hajek, „Dynamic Behavior Modeling and Verification of Advanced Electrical-Generator Set Concept" IEEE Transactions on Industrial Electronics, January, 2009, vol. 56, nr:1, pp. 266-279

[6] C. Sourkounis, J. Wenske, „Cascaded State Control for Dynamic Power Conditioning in Wind Parks", Proceeding of the International Conference on Electrical Power Quality and Utilisation, EPQU 2011, Lisbon, 17 October 2011 through 19 Ocotber, 2011

[7] A. El Aroudi, B. Robert, A. Cid-Pastor, L. Martinez-Salamero, „Modeling and Design Rules of a Two-Cell Buck Converter Under a Digital PWM Contoller" IEEE Transactions on Power Electronics, 2008, Vol 23, Issue 2, pp. 859-870

[8] P.M. Lacko M. Olejar, J. Dudrik, „DC-DC Push – Pull Converter with Turn-Off Snubber for Renewable Energy Sources", EDPE 2009, Dubrovnik, Croatia, 12-14 Oct, 2009, CD Rom ISBN: 953- 6037-56-8

[9] C. Sourkounis, J. Wenske, "Electronic synchronous machine for dynamic power conditioning in wind parks", Compability and Power Electronics (CPE 2011), Tallin, Estonia, 1-3 June, 2011, pp. 56-61, *ISBN: *978-1-4244-8805-6,

[10] Mohammad N. Marwali, Jin-Woo Jung, Ali Keyhani "Control of Distributed Generation Systems- Part II: Load Sharing Control" IEEE Transaction on Power Electronics, USA, November, 2004, Vol.19, No 6., pp. 1551-1651

[11] J. Enslin, Zhenyu Fan, Pavol Bauer "Principles and Issues Relating to the Interconnection of Wind Power", PCIM 2005, Nürnberg, Germany, 7-9 June, 2005, CD Rom ISBN: 3-928643-41-x

[12] T. Ghennam, EM. Berkouk, B. Francois, K. Aliouane, "A New Space-Vector

[13] Based Hysteresis Current Control Applied on Three-Level Inverter to Control Active and Reactive Powers of Wind Generator" International Conference on Power Engineering, Energy and Electrical Drives, 2007. POWERENG 2007, pp. 636-641

[14] Li Hui Yang, Zhao Xu, Østergaard, J, Zhao Yang Dong, Xi Kui Ma, "Hopf bifurcation and eigenvalue sensitivity analysis of doubly fed induction generator wind turbine system", Power and Energy Society General Meeting, 2010 IEEE, Minneapolis, MN, pp. 1-6, 25-29 July, 2010, ISBN:978-1-4244-6549-1,